Chimie Douce Route to Sodium Hydroxo Titanate Nanowires with Modulated Structure and Conversion to Highly Photoactive Titanium Dioxides

Chih-Wei Peng,[†,‡] Mireille Richard-Plouet,[†] Tsung-Yin Ke,[§] Chi-Young Lee,[*,§] Hsin-Tien Chiu,[‡] Christiane Marhic,[†] Eric Puzenat,[||] Frederic Lemoigno,[⊥] and Luc Brohan[*,†]

Institut des Matériaux Jean Rouxel (IMN), Université de Nantes, CNRS, 44322 Nantes, France, Department of Applied Chemistry, National Chiao Tung University, Taiwan 30050, R. O. C., Department of Materials Science and Engineering and Center for Nanotechnology, Materials Science and Microsystems, National Tsing Hua University, Taiwan 30043, R. O. C., Institut de recherches sur la catalyse et l'environnement de Lyon, CNRS, Université Lyon 1, 69622 Villeurbanne, France, and Institut Charles Gerhardt (CTMM), UMII-UMI-CNRS-ENSCM, Université Montpellier II, 34095 Montpellier, France

Received March 10, 2008. Revised Manuscript Received September 30, 2008

Sodium hydroxo titanate nanowires with $NaTi_2O_4(OH)$ formulation are fabricated by chimie-douce from TiO_2 powders in a hot concentrated base solution. In the present work, we investigate, in detail, the structure and morphology of the titanate, acid-exchanged materials, and phases formed during dehydration of these compounds; we then discuss the relationship between the initial titanate structure and TiO_2 formation. XRD, ED, HRTEM, EDS, density measurements, and TG/MS results suggest that the titanate and acid-exchanged structures were closely related to the pseudolepidocrocite arrangement ("$Cs_2Ti_6O_{12}$" type). The average structure of $NaTi_2O_4(OH)$ nanowires consists of noncorrugated $Ti_2O_3(OH)$ and NaO layers stacked along the [010] direction and an energy minimization was further conducted by theoretical methods. From TEM study, we demonstrated that $NaTi_2O_4(OH)$ exhibits a modulated structure (q wave vector equals to 1/7 [001]*), which originates from the misfit between the NaO and $Ti_2O_3(OH)$ sublattices. $NaTi_2O_4(OH)$ structure has a monoclinic distortion (*I*2/*m* space group) with refined unit cell $a = 0.37000(6)$ nm, $b = 1.7816(4)$ nm, $c = 2.2077(3)$ nm, $\beta = 92.70(1)°$. Proton exchange followed by heat treatment convert the sodium hydroxo titanate into highly photoactive TiO_2 nanowires. The activity is attributed to the presence of preferentially exposed (001) surface plane which is explained by the topotactic phase transformation of TiO_2(B) into anatase.

1. Introduction

Because of the potential applications in the fields of energy conversion and environmental protection, the photochemistry of TiO_2 is a fast growing area both in terms of research and commercial activity.[1,2] In such applications, the performance of titanium oxide can be optimized with specific nanostructural control over the morphology of the material. A. Selloni et al. reported lately that the dissociation of water spontaneously occurs on (001) and defected (101) surfaces of anatase TiO_2 according to the calculated results.[3] This implies that Titanium oxide nanomaterials with preferred orientation and high active site density on the (001) and (101) surfaces could significantly enhance the photocatalytic efficiency. Recently, various titanium oxide nanowires[4−6] and nanotubes,[7,8] with preferred orientations, have been synthesized from sodium titanate via chimie douce (soft chemistry) routes. Among them, TiO_2(B) nanowires, exhibiting excellent photocatalytic efficiency, even better than P25 Degussa and commercial anatase, have been synthesized.[9] In literature, numerous methods have been reported for the synthesis of sodium titanate nanowires with complex structures.[4−6,9−11,15] Many of them,[9−14] have been converted into titanium dioxide under

* Corresponding author. E-mail: luc.brohan@cnrs-imn.fr (L.B.); cylee@mx.nthu.edu.tw (C.-Y.L.).
[†] Université de Nantes.
[‡] National Chiao Tung University.
[§] National Tsing Hua University.
[||] Université Lyon 1.
[⊥] Université Montpellier II.

(1) Mills, A.; Lee, S.-K. *J. Photochem. Photobiol., A* **2002**, *152*, 233.
(2) Carp, O.; Huisman, C. L.; Reller, A. *Prog. Solid State Chem.* **2004**, *32*, 33.
(3) (a) Vittadini, A.; Selloni, A.; Rotzinger, F. P.; Grätzel, M. *Phys. Rev. Lett.* **1998**, *81*, 2954. (b) Gong, X.-Q.; Selloni, A. *J. Phys. Chem. B* **2005**, *109*, 19560. (c) Gong, X.-Q.; Selloni, A.; Batzill, M.; Diebold, U. *Nat. Mater.* **2006**, *5*, 665.
(4) Yuan, Z.-Y.; Colomer, J.-F.; Su, B.-L. *Chem. Phys. Lett.* **2002**, 362.
(5) Armstrong, A. R.; Armstrong, G.; Canales, J.; Bruce, P. G. *Angew. Chem., Int. Ed.* **2004**, *43*, 2286.
(6) Yoshida, R.; Suzuki, Y.; Yoshikawa, S. *J. Solid State Chem.* **2005**, *178*, 2179.
(7) Kasuga, T.; Hiramatsu, M.; Hoson, A.; Sekino, T.; Niihara, K. *Adv. Mater.* **1999**, *11*, 1307.
(8) Armstrong, G.; Armstrong, A. R.; Canales, J.; Bruce, P. G. *Chem. Commun.* **2005**, 2454.
(9) Dong, W.; Cogbill, A.; Zhang, T.; Ghosh, S.; Tian, Z. R. *J. Phys. Chem. B* **2006**, *110*, 16819.
(10) Zhu, H.; Gao, X.; Lan, Y.; Song, D.; Xi, Y.; Zhao, J. *J. Am. Chem. Soc.* **2004**, *126*, 8380.
(11) Wu, D.; Liu, J.; Zhao, X.; Li, A.; Chen, Y.; Ming, N. *Chem. Mater.* **2006**, *18*, 547.
(12) Ma, R.; Fukuda, K.; Sasaki, T.; Osada, M.; Bando, Y. *J. Phys. Chem. B* **2005**, *109*, 6210.

10.1021/cm8007039 CCC: $40.75
Published on Web 11/05/2008

appropriate reaction conditions.[13,14] However, the exact structures of the titanates remain largely misunderstood. Several standard structural models have been proposed as assumed intermediates, namely layered titanates such as $Na_2Ti_4O_9$, $Na_2Ti_3O_7$, or lepidocrocite types. Zhu et al. proposed that the structure of the nanowire is a lamellar arrangement as in the tetratitanate structure,[10] whereas Wu et al. suggested that nanowires are composed of trititanate units.[11] A lepidocrocite structure, with infinite zigzag chains, has also been assigned as nanowire constituent.[12−16] More understanding of the structure of titanate nanowires may be helpful to comprehend their growth mechanism and to provide tailored synthesis of TiO_2 with enhanced properties. In this work, we report a thorough structural characterization of sodium titanate nanowires prepared by a chimie douce method. Further processing of the nanowires generates TiO_2(B) and anatase TiO_2 nanowires. We found that this anatase nanowires with highly (001)-exposed shows enhanced photocatalytic activity better than Degussa P25 TiO_2, which is the currently reported best commercial photocatalyst. This result strongly supports the theoretical predictions provided by A. Selloni.[3]

2. Experimental Section

Preparation of $NaTi_2O_4(OH)\cdot xH_2O\cdot yCO_2$ A. Titanate nanowires were synthesized by adding TiO_2−anatase (1.0 g, Riedel-de-Haën) or amorphous TiO_2 (1.0 g, synthesized from $TiOCl_2$ hydrolysis by excess NH_4OH) to a 10 mol.L^{-1} aqueous solution of NaOH (10 mL). The mixture was transferred to a Teflon-lined (50 mL) autoclave and heated to 453 K for 24−72 h. The material was washed with distilled water then filtered. The steps were repeated until pH becomes lower than 12. After centrifuging and drying at 343 K in air, **A** (1.3 g) was isolated.

Preparation of $NaTi_2O_4(OH)\cdot xH_2O\cdot yCO_2$ B. To NaOH(aq) (10 mol L^{-1}, 30 mL) in a 300 mL PTFE round-bottom flask equipped with a coil condenser was added amorphous TiO_2 (1.0 g, synthesized from $TiOCl_2$ hydrolysis by excess NH_4OH). The mixture was refluxed in an air atmosphere at 423 K (oil bath temperature) for 72 h. **B** (1.3 g) was isolated via the analogous workup procedure mentioned above.

Preparation of $HTi_2O_4(OH)\cdot xH_2O\cdot yCO_2$ HA and HB. The **A** (1.0 g), product was acid-washed, which involved stirring the sample in 0.1 mol L^{-1}, HNO_3(aq) solution (50 mL) for 2 h. The material was then filtered, washed with distilled water, and collected by centrifuging repeatedly until pH is above 6. After being dried in an oven at 343 K under air, **HA** (0.8 g) was obtained. **HB** can be prepared by using the same process.

Preparation of TiO_2(B) HA-1 and HB-1. TiO_2(B) nanowires, **HA-1** and **HB-1**, were prepared by heating the acid-washed titanate nanowires, **HA** and **HB**, respectively, at 673 K (rate, 10 K min^{-1}), for 4 h in air.

Preparation of Anatase TiO_2 HA-2 and HB-2. Subsequent thermal treatment of **HA** and **HB** at 1073 K (rate, 10 K min^{-1}) for 4 h in air, converts them to **HA-2** and **HB-2**, respectively.

Preparation of Sodium Titanate, Titanic Acid, and TiO_2 Nanotubes. Titanate nanotubes were synthesized by adding TiO_2-anatase (1.0 g, Riedel-de-Haën) to a 10 mol L^{-1} aqueous solution of NaOH (10 mL). The mixture was transferred to a Teflon-lined (50 mL) autoclave and heated to 423 K for 24−72 h. The material was washed with distilled water following a procedure similar to that of the **A** preparation and then filtered. For preparation of titanic acid and TiO_2 nanotubes, the above isolated powder was treated in a process similar to that of **HA** and **HA-1** preparation, respectively.

Characterization. SEM images were obtained by using a JEOL 6400F with a tungsten cathode field emission gun operating at 10 keV. XRD data were collected on a Siemens D5000 diffractometer with the Cu Kα radiation in a Bragg−Brentano geometry. TEM studies were performed on a Hitachi HF2000 with a field emission electron source at 200 keV. Samples prepared by grinding solid products followed by dispersing them in ethanol were placed on holey or lacey carbon films on copper grids for TEM studies. TEM simulations were performed using a specialized program "Mac Tempas",[17] which uses parameters of the structures, including cell parameters, space group, atom positions, thickness, and defocalization. EDX studies were performed by using a PGT X-ray analysis probe attached to a JEOL 5800LV SEM with a conventional tungsten electron source operating at 15 keV. The EDX samples were prepared by pressing 100 mg of powder into a pellet with 8 mm diameter and 1−2 mm thickness. The signal was collected from a well-planar surface to limit the differential absorption phenomenon. In addition, a standard sample NaCl is used to carefully calibrate the detector and the decomposition procedure. In that case, the accuracy was estimated lower than 3% for the Na/Ti molar ratio. TGA-MS studies were carried out using a SETARAM TG-DSC 111 equipment fitted with Mass Spectrometer facility (Leybold Inficon) operating at 273−1073 K with a heating rate of 5 K/min, in Ar environment. FT-IR spectra were observed using a Bruker Vertex 70 equipped with a universal attenuated total reflection (ATR) accessory (Golden Gate™ Single Reflection Diamond ATR). FT-Raman studies were performed on a Bruker RFS100 equipped with a 1064 nm infrared laser as the incident light, which allows one to focus a sample area with a diameter less than 1 mm. The specific surface area determined from the Brunauer−Emmett−Teller equation (BET method) was performed by N_2 adsorption at 77 K (under liquid nitrogen) using the adsorption apparatus Micromeritics ASAP 2010 instrument. The density measurements were carried out at room temperature by means of an ACCUPYC 1330 Pycnometer (Micromeritics) with a high accuracy (for a total volume of 1 mL, ΔV is lower than 1 μL). Before the measurements, all compounds were treated in an oven at 423 K for one day.

Photocatalytic Study. Photodecomposition of methylene blue was used to test photocatalytic efficiency of the titanium dioxides prepared in this study. Irradiation was provided by a Xe lamp (Osram 180W). Photocatalytic tests were performed at room temperature. For each test, TiO_2 (10 mg) was added, under stirring, to an aqueous solution of methylene blue (25 ppm, 20 mL). A sample (0.5 mL) was taken from the suspension at a designed time interval for analysis. The methylene blue concentration of samples was determined by Hitachi U3010 UV−vis photospectrometer.

Computational Parameters. Crystal structure of phase **A** has been relaxed with the Density Functional Theory (DFT) code VASP.[18] In this code, atoms are represented by plane waves in the Plane Augmented Waves (PAW) formalism.[19] We used the Generalized Gradient Approximation (GGA) with the Perdew, Burke, Ernzerhof (PBE) functional for exchange and correlation

(13) Tournoux, M.; Marchand, R.; Brohan, L. *Prog. Solid State Chem.* **1986**, *17*, 33.
(14) Feist, T. P.; Davies, P. K. *J. Solid State Chem.* **1992**, *101*, 275.
(15) Meng, X.; Wang, D.; Liu, J.; Zhang, S. *Mater. Res. Bull.* **2004**, *39*, 2163.
(16) Tsai, C.; Teng, H. *Chem. Mater.* **2006**, *18*, 367.
(17) O'Keefe, M. A.; Kilaas, R. *MacTempas, V1.70 and Crystalkit V1.77, HRTEM Image Analysis*; Lawrence Berkley National Laboratory: Berkeley, CA, 1987.
(18) (a) Kresse, G.; Hafner, J. *Phys. Rev. B* **1993**, *47*, 558. (b) Kresse, G.; Furthmuller, J. *Comput. Mater. Sci.* **1996**, *6*, 15.
(19) Kresse, G.; Joubert, D. *Phys. Rev. B* **1999**, *59*, 1758.

Table 1. Summary of Sample Preparation and Their Morphological Properties

sample	precursor	preparation	morphology	dimension (width/length (nm))	phase	specific surface ($m^2\ g^{-1}$)
A	RDH TiO_2 *d*: 100 − 300 nm	10 M $NaOH_{(aq)}$, *453 K*, 48 h in autoclave	fibrous	50−200/500−5000	lepidocrocite: "$Cs_2Ti_6O_{12}$"-type	27
HA	**A**	0.1 M $HCl_{(aq)}$, 298 K, 2 h	fibrous	50−200/500−5000	lepidocrocite: "$Cs_2Ti_6O_{12}$"-type	52
HA-1	**HA**	673 K, 4 h	fibrous	50−200/100−5000	TiO_2(B)	41
HA-2	**HA**	1073 K, 4 h	fibrous	50−200/100−2000	anatase	13
B	amorphous TiO_2[a]	reflux in 10 M $NaOH_{(aq)}$, 48 h	fibrous	10−40/50−1000	lepidocrocite: "$Cs_2Ti_6O_{12}$"-type	35
HB	**B**	0.1 M $HCl_{(aq)}$, 298 K, 2 h	fibrous	10−40/50−1000	lepidocrocite: "$Cs_2Ti_6O_{12}$"-type	105
HB-1	**HB**	673 K, 4 h	fibrous	10−40/50−1000	TiO_2(B)	71
HB-2	**HB**	1073 K, 4 h	fibrous	10−40/50−1000	anatase	25
nanotube	RDH TiO_2 *d*: 100 − 300 nm	10 M $NaOH_{(aq)}$, *423 K*, 48 h in autoclave	tubular	5−10/50−300	sodium titanate	262
H nanotube	nanotube	0.1 M $HCl_{(aq)}$, 298 K, 2 h	tubular	5−10/50−300	less-ordered titanic acid	284
TiO_2 nanotube	H-nanotube	673 K, 4 h	fibrous	5−10/10−100	anatase + TiO_2(B)	323
Degussa P25			particle	30	anatase + rutile	50

[a] synthesized from hydrolysis of $TiOCl_2$ in excess NH_4OH.

energy.[20] The convergence of the calculations was checked with respect to both energy cutoff (up to 700 eV) and k-point grid sampling (up to 5 × 2 × 5 Monkhorst-Pack mesh) in order to achieve reliable converged structure.

3. Results and Discussion

The treatment of TiO_2 precursors in NaOH solution was conducted either in autoclave or refluxing conditions, which produced **A** and **B** compounds respectively. The **HA** and **HB** samples, in which Na^+ ions were fully exchanged by protons, were obtained by washing **A** and **B** in diluted acidic solutions. Finally, annealing of **HA** and **HB** at 673 K led to **HA-1** and **HB-1**, respectively. Upon calcinations of **HA** and **HB** at 1073 K, **HA-2** and **HB-2** were isolated, correspondingly. Detailed experimental conditions for samples preparation and morphological properties are summarized in Table 1.

3.1. Morphology Study by SEM. A scanning electron microscopic (SEM) image in Figure 1a shows that **A** is composed of nanowires with diameters 50 − 200 nm and lengths 0.5 − 5 μm. Apparently, the morphology of **A** is mostly retained in **HA** (Figure 1b). Close examination of the sample suggests that it is more fragmented than **A**. The fragmentation is more evident in **HA-1** (Figure 1c). After post-treatment at 1073 K, the form-factor (length to width aspect ratio) of **HA-2** further decreased. In Figure 1d, the nanowires in **HA-2** show almost the same diameters as in **HA** but their lengths decrease to 0.1−1 μm. **HA-2** will be denoted nanorods hereafter. Sample **B**, obtained in refluxing conditions at 423 K, is composed of small nanowires with diameters 10−40 nm and lengths 0.05−1 μm as shown in Figure 1e. Further post-treatments of **B** led to the formation of **HB**, **HB-1**, and **HB-2** (Figure 1f). They exhibit a morphology variation trend analogous to that observed for the samples treated from **A**. In both cases, increasing reaction duration increased the lengths of the nanowires only. The diameters essentially remained the same. This observation is in agreement with previous reports.[6,9]

3.2. Composition Determination. Using an energy-dispersive X-ray (EDX) analyzer attached to the SEM, we found that **A** and **B** contained a significant amount of Na, with Na/Ti ≈ 0.52, whereas **HA** and **HB** were essentially Na free. The IR spectra of **A**, **B**, **HA**, and **HB** showed absorptions from vibrations of O−H and Ti−O bonds (Figure S1 in the Supporting Information). In addition, the spectra of **A** and **B** displayed C−O bands, which are assigned to the presence of carbonate groups, $\nu C{-}O_I$ and $\nu\ C{-}O_{II}$ at 1380 and 1680 cm^{-1}, respectively. For **HA** and **HB**, intensities of the carbonate bands were much weaker, whereas the OH bands remained unchanged. The $\nu C{-}O_I$ vibration attributed to unidentate carbonates is no more observed. This probably was the result of the acidification of **A** and **B**. Thermogravimetric analysis/mass spectrometry (TGA/MS) was undertaken to estimate the quantity of the bonded hydroxyl and carbonate groups, and the adsorbed water molecules in the samples (Figure S2 in the Supporting Information). For all samples, two water departures below

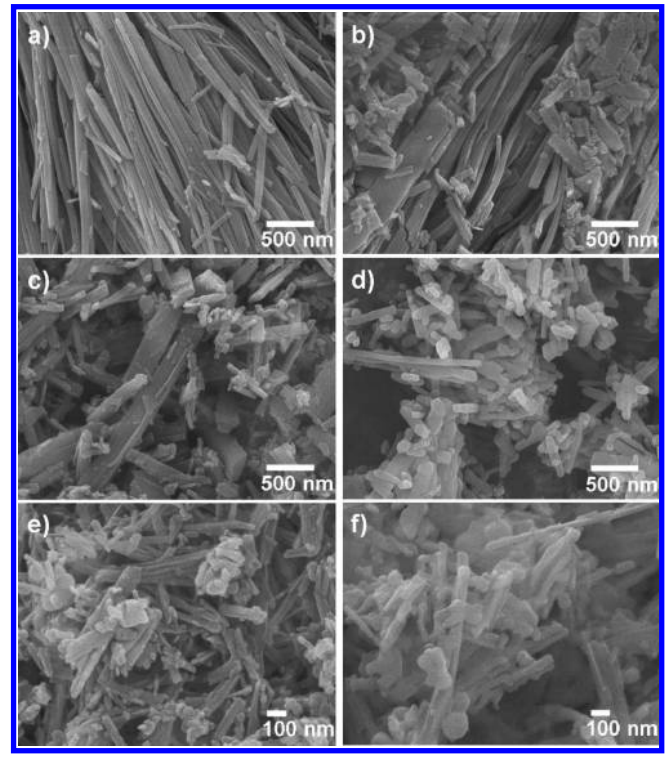

Figure 1. SEM images of (a) **A**, (b) **HA**, (c) **HA-1**, (d) **HA-2**, (e) **B**, and (f) **HB-2**.

(20) Perdew, J. P.; Burke, S.; Ernzerhof, M. *Phys. Rev. Lett.* **1996**, *77*, 3865.

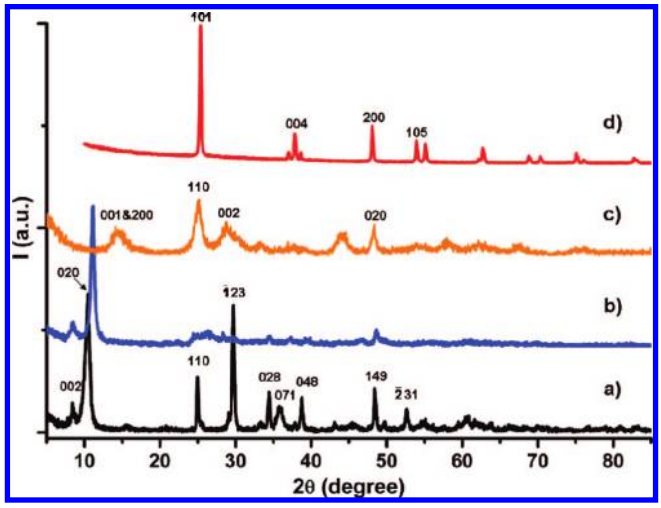

Figure 2. XRD patterns of (a) **A**, (b) **HA**, (c) **HA-1**, and (d) **HA-2**.

423 and 673 K are detected through a peak corresponding to *m*/*z* 18 (*m*, mass; and *z*, charge). This water release is attributed to the condensation of the Ti-OH groups from 2D to 3D structure. The departure of species with *m*/*z* 44 (CO_2) appeared below 423 K and between 873 and 1073 K. These are assigned to the decomposition of unidentate and multidentate carbonates, respectively. On the basis of the EDX and the TGA/MS results, chemical composition of **A** and **B** can be expressed as a sodium hydroxo titanate $NaTi_2O_4(OH)$. It also contained a small amount of adsorbed species which can be formulated as "$xH_2O \cdot yCO_2$" ($x = 0.4-0.6$, $y = 0.02-0.36$). Likewise, the empirical formulas of **HA** and **HB** were determined to be "$HTi_2O_4(OH) \cdot xH_2O \cdot yCO_2$" ($x = 0.4-0.6$, $y = 0.01-0.06$).

3.3. Structural Characterizations. *3.3.1. XRD and Raman Studies.* In Figure 2, the XRD patterns of both A and HA exhibit a strong reflection peak occurring at large spacing distance about 1.0 nm, suggesting that their framework might be related with the layered titanates characterized below. It is well-known that related alkali titanates $A_2Ti_nO_{2n+1}$ (A: alkali ion), exhibit layered ($3 \le n \le 5$) and tunnel ($n \ge 6$) arrangement and form a homologous series of monoclinic structures.[21] The host lattice of these alkali titanates are built up from zigzag ribbons of octahedra sharing edges that run along the *b* axis. Here, these closely related compounds are described as long period structures derived from $Cs_{0.33}TiO_2$, (denoted "$Cs_2Ti_6O_{12}$").[22−24] The $M_x(Mg_{x/2}Ti_{1-x/2})O_2$ titanates with M = Ba, Tl[25,26] and "$Cs_2Ti_6O_{12}$" bronze can be considered as particular layered compounds with layers, containing only one ribbon of infinite length, like in lepidocrocite type γ-FeO(OH).[27] The main difference between both structures originates from the relative stacking of the ribbons (along the [010] direction), which is built up from antiphased layers along the *a* axis for "$Cs_2Ti_6O_{12}$" type, instead of phased layers in lepidocrocite (Figure S3 in the Supporting Information). Referring to the rock-salt structure, "$Cs_2Ti_6O_{12}$" can be described as a periodic stacking of three layered sublattices, i.e., [□][□], [□]O, and TiO, along [010] in which the Cs atoms occupied the oxygen vacancy sites (noted □). In terms of NaCl-type, the deduced composition is written $[Ti_2□_3][O_4□]$. Although possible structures of chimie douce titanate nanowires have been proposed to possess (*C*2/*m* or *P*2/*m*) monoclinic alkali titanates $Na_2Ti_4O_9$ or $Na_2Ti_3O_7$ structures, the XRD results did not match well with the known data.[11,12] The agreement with the Raman data is also not in favor of the tetra- or trititanate. The peak observed at 910 cm^{-1} is indeed assigned to a dangling Ti−O sticking out into the interlayer space,[15] in a stepped layer structure. Here (Figure S4 in the Supporting Information), this peak is hardly marked and this observation implies that the structures are similar to a noncorrugated layer or a tunnel structured titanates. All the evidence reveals that A does not have a typical stepped layer structure. Therefore, we propose that a structural model for **A** could derive from a noncorrugated layered structure closely related to "$Cs_2Ti_6O_{12}$". Detailed structural description for **HA** will be discussed in section 3.3.4. The XRD patterns of **HA-1** and **HA-2** in Figure 2 suggest that the allotropic variety is TiO_2(B) and anatase phases, respectively. Additional structural features of both **HA-1** and **HA-2** will be described in *3.3.4.* too. The patterns of **B**, **HB**, **HB-1**, and **HB-2** (see Figure S5 in the Supporting Information) exhibit almost the same peak positions and relative intensities, but a broadening in peak widths was detected, as those of the corresponding samples developed from **A**.

3.3.2. TEM Studies of $NaTi_2O_4(OH)$. Figure 3a shows a low magnification transmission electron microscopic (TEM) image of A, showing bundles of nanowires with apparent diameters of tenths of μm and lengths of several μm. From a separated nanowire in Figure 3a, a high-resolution (HR) image in Figure 3b is obtained. Figure 3c is the filtered image of Figure 3b. The white rectangular area in Figure 3c represents the centered unit cell observed along [010]. In Figure 3b, the distance between the repeating fringe units is 1.1 nm, which significantly differs from stepped-layer unit evidenced in tetra-titanate (1.2 nm) or trititanate (0.9 nm). The selected area electron diffraction (SAED) of A along [010] (Figure 3d) gives evidence for two main characteristic distances 0.37 and 0.315 nm with the following reflection conditions (h00): $h = 2n$, (00 *l*): $l = 2n$, (*h*0*l*): $h + l = 2n$. These observations are not in agreement with the space group extinctions of the stepped layer structures such as $Na_2Ti_4O_9$ (*C*2/*m*, reflection condition $h + k = 2n$) or $Na_2Ti_3O_7$ (*P*2/*m*, no special reflection condition) but are similar to those observed in the orthorhombic bronze, $Cs_2Ti_6O_{12}$ (*Imm*2), which has a noncorrugated layer structure. The (010) reciprocal plane analysis reveals a slightly distorted cell with an angle equal to $\beta^* \approx 87°$, which suggests a monoclinic distortion with an I mode. Besides this, a reinforcement of the intensity every 7 spots can be seen on the ED pattern, along the [001]* direction. The existence of six satellites peaks along [001]* suggests a structural modulation in which

(21) (a) JCPDS number 32−0681; (b) JCPDS number 33−1294; (c) JCPDS number 38−0172.
(22) Le Granvalet-Mancini, M.; Brohan, L.; Marie, A. M.; Tournoux, M. *Eur. J Solid State Inorg. Chem.* **1994**, *31*, 767–777.
(23) Le Granvalet-Mancini, M.; Marie, A. M.; Roucau, C.; Caldes, M.; Brohan, L. *Microsc. Microanal. Microstruct.* **1997**, *8*, 203.
(24) Grey, I. E.; Madsen, I. C.; Watts, J. A.; Bursill, L. A.; Kwiatkowska, J. *J. Solid State Chem.* **1985**, *58*, 350.
(25) Dryden, J. S.; Wadsley, A. D. *J. Chem. Soc., Faraday Trans.* **1958**, *54*, 1574.
(26) Verbaere, A.; Dion, M.; Tournoux, M. *Rev. Chim. Miner.* **1975**, *12*, 156.
(27) Oles, A.; Szytula, A.; Wanic, A. *Phys. Status Solidi* **1970**, *41*, 173.

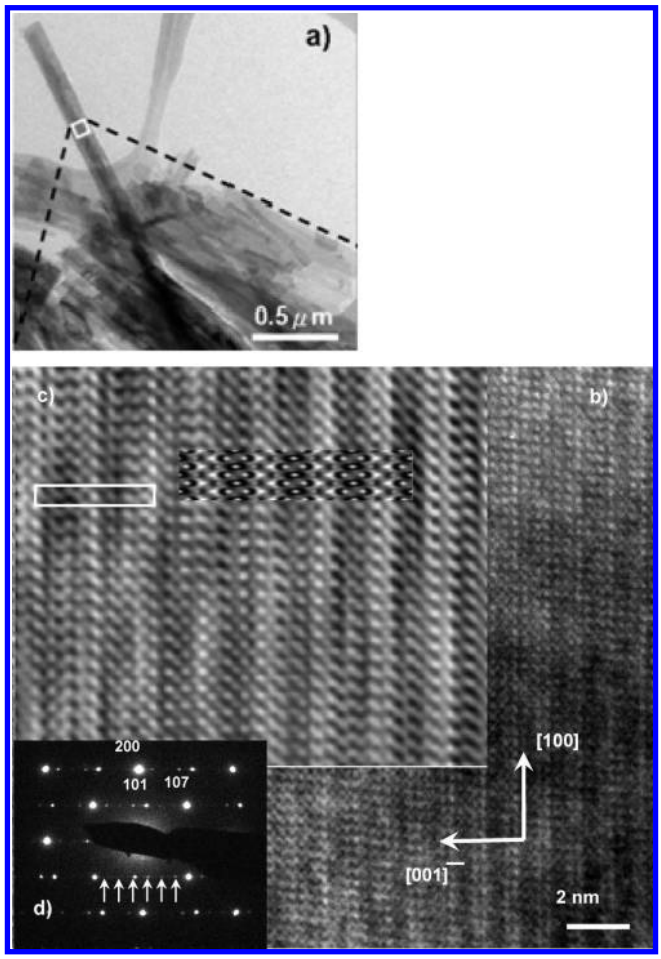

Figure 3. TEM studies of **A**: (a) Low-magnification image; (b) high-resolution image along [010] of the selected area marked as white square in (a); (c) filtered high-resolution image b; insets, representative unit cell marked as a white rectangle and HRTEM simulated Image (defocus −90 nm, thickness 34 nm); (d) selected area electron diffraction pattern viewed along [010] (white arrowheads indicate the satellite peaks position).

the q wave vector equals $1/n$ [001]*. The lattice parameter of the superstructure is then $c = nc'$, i.e., $7 \times 3.15 \approx 2.2$ nm, where c' is close to the c parameter of "$Cs_2Ti_6O_{12}$" unit cell, 0.2981(2) nm. TEM and XRD analysis show that A crystallizes in a monoclinic system, *I*2/*m* space group, with the following refined cell parameters $a = 0.37000(6)$ nm, $b = 1.7816(4)$ nm, $c = 2.2077(3)$ nm, $\beta = 92.70(1)°$. The refinement was conducted using Jana 2000.[28] The peak position and intensity of the experimental and the refined XRD patterns with reliability factors are summarized in the Supporting Information (Figure S6 and Table S1).

To support this analysis, we modeled the structure of $NaTi_2O_4(OH)$ to be analogous to that of "$Cs_2Ti_6O_{12}$", preserving the TiO framework. Cell parameters and atomic positions were fully relaxed starting from the XRD refinement results, with a force convergence criterion of 5×10^{-3} eV Å^{-1}. The relaxed structure is in remarkable agreement with the averaged pseudolepidocrocite structure since we obtained the following cell parameters $a = 0.364$ nm (1.58%), $b = 1.729$ nm (2.97%), $c = 0.302$ nm (3.96%), $\alpha = 91.2°$, $\beta = 89.9°$ and $\gamma = 88.2°$ (relative errors with respect to the XRD parameters are reported in parenthesis). Relative error for cell parameters remains below 4% and it is worth noting that the highest discrepancy between experimental and calculated cell parameters is for c parameter that is in the direction of the structural modulation. The position of atoms in the proposed structure is only preliminary (see the Supporting Information, Table S3) and further calculation of energy minimization and XRD refinement will be necessary to take into account the modulation.

(28) Petricek, V. *The Crystallographic Computing System JANA2000*; Institute of Physics: Prage, Czech Republic, 2000.

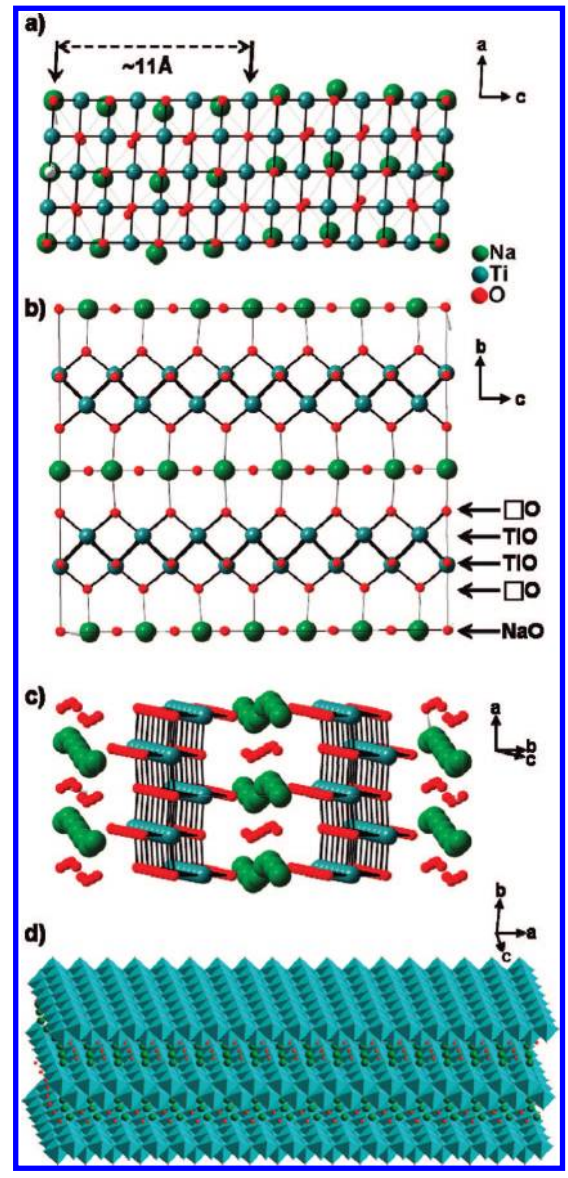

Figure 4. Structural model for the sodium hydroxo titanate **A**, derivative of the pseudolepidocrocite, $Cs_2Ti_6O_{13}$: (a) viewed along the *b* axis, (b) viewed along the *a* axis, (c) viewed along [1 1 10], and (d) viewed along [$\bar{2}$12] displaying 3D feature of linked TiO_6 octahedra.

3.3.3. Modulated Layer Structure of $NaTi_2O_4(OH)$. Assuming that the misfit between NaO and TiO sublattice distances causes the observation of six satellite peaks on the ED pattern along [001]*, we can propose the structural model shown in Figure 4. This assumption is corroborated by the fact that the sodium hydroxide (NaOH noted hereafter SH) structure, in beta form, also contains rock-salt subunits with a periodicity $a_{SH} = 0.3345(3)$ nm and $b_{SH} = 0.3445(3)$ nm in the (110) plane.[29] Compared to the TiO lattice $a = 0.3821(3)$ nm, $c = 0.2981(2)$ nm in "$Cs_{2Ti_6O_{12}}$", and without

any accommodation of this misfit, the Na−O lattice is in tension in the $[100]_{\text{“}Cs_2Ti_6O_{12}\text{”}}$ direction whereas it is compressed in the $[001]_{\text{“}Cs_2Ti_6O_{12}\text{”}}$ direction. One possibility to accommodate the misfit is to displace the Na and O atoms along the *a* axis in the (*a*, *c*) plane (Figure 4a−c). This misfit could be reduced if a sinusoidal distortion of the Na and O atoms is applied into the (101) plane to accommodate the Na−O distances at 0.337−0.344 nm values. Along the *c*-axis, the sequence repeats every seven regular Ti−O sublattices which becomes in coincidence with the distorted Na−O sublattice. Such a model is coherent with the seventh order superstructure found in the [010]* zone axis in Figure 3d. These results give evidence that the $NaTi_2O_4(OH)$ nanowires exhibit a commensurate modulated structure along the [001] direction. Figure 4d shows the proposed structural model along the $[\bar{2}12]$ direction. This representation gives an idea of the crystalline directions that are preferentially developed during the nanowire growth.

For further comparison of the assumed structure and the TEM observations, Mac Tempas simulation of ED (see Figure S10 in the Supporting Information) and HRTEM patterns were performed on an idealized structural model of a monoclinic system with *I*2/*m* space group. As shown in Figure S10b, the peaks intensity and position of the simulated ED pattern, viewed along [010]*, qualitatively agree with the experimental result. In Figure 3c, the HRTEM image simulated from the idealized model (focal −90 nm; thickness 34 nm) viewed along [010] has been found to superimpose well on the observed image. The modeled structure is coherent with the other experimental results: EDX chemical composition analysis, theoretical and experimental densities ($d_{calcd} = 3.20$; $d_{obsd} = 3.17(2)$) and weight loss measured by thermogravimetric analysis.

3.3.4. Characterization of $HTi_2O_4(OH)$, $TiO_2(B)$, and Anatase TiO_2. As shown in Figure 2, the XRD pattern of **HA** is slightly different from that of **A**. In particular, only the most intense peaks are still present in **HA**, the product acidified from **A**, whereas the peak widths are broader than those of **A**. Referring to the previous indexations of **A** and assuming a layered structure for the fully proton exchanged titanate, the two main peaks of **HA** are identified as (002) and (020) (interlayer spacing). In a first approximation, the refined parameters $a = 0.37405(2)$ nm, $b = 1.6744(4)$ nm, $c = 2.2143(2)$ nm, $\beta = 92.70(1)°$ indicate a significant contraction of the interlayer spacing while the other parameters are slightly changed. Such behavior is in agreement with that usually observed for acid exchanged titanates.[13,14] The peak position and intensity of the experimental and the refined XRD patterns with reliability factors are shown in the Supporting Information (Figure S6 and Table S2).

On the basis of XRD and TEM results, it appears that **HA-1** crystallizes as TiO_2(B) nanowires (Figure 2c, 5a, and 5b) and convert into **HA-2** anatase nanowires, after annealing at 1073 K (Figures 2d, 5c, and 5d). **B**, **HB**, **HB-1**, and **HB-2** (Figure S5 in the Supporting Information), exhibit analogous structures to **A**, **HA**, **HA-1**, and **HA-2** (Figures 2 and S6), but anatase shows inherent particles size differences that impact the photocatalytic properties (see below). The shape and size of the nanocrystallites vary with the preparation techniques and procedures. Factors such as ionic strength, nature of the ligand (aquo, oxo, or hydroxo) at the surface of the reactant (amorphous or crystalline precursor), thermal treatment (autoclave (**A**), reflux (**B**)), and in addition, the nature of adsorbed species (HCO_3^-, CO_3^{2-}) strongly impact on the final form of materials. Typically, (101) and (001) surface planes are found in P25 powder materials, together with some (100)/(010). The anatase nanowires, obtained by “chimie douce”, mainly exhibit (001) surface plane and a growing axis along the [010] direction is observed in TEM images. To quantify the preferential orientations, we performed an analysis of the X-ray diffraction peaks (Figure S8 in the Supporting Information). The XRD peak intensities of **HA-2**, **HB-2**, **P25**, **TiO_2-tube** are summarized in Table S4 of the Supporting Information with calculated intensities of randomly oriented anatase (JCPDS 89−4921, calculated intensities). For comparison, all the intensity values were normalized to the (112) peak intensity of nonoriented anatase, denoted reference or ref, in the following. The preferential orientation can be estimated through the ratio between the XRD peak intensities of the samples to the same peak intensities of the reference, $I_{(hkl)}/I_{(hkl)ref}$ (see Table 2). The $I_{(101)}/I_{(101)ref}$, $I_{(004)}/I_{(004)ref}$ and $I_{(200)}/I_{(200)ref}$ ratios for **HA-2** (autoclave) and **HB-2** (reflux) are stronger than that of P25. Therefore, the anatase nanowires, converted from the titanate nanowires, expose more (101), (001), and (100) planes than the other samples. In comparison to **HA-2**, **HB-2** shows a higher (004) peak intensity, whereas their respective (101) and (200) intensities are almost the same. The preferential orientation in the (001) plane and consequently the increased

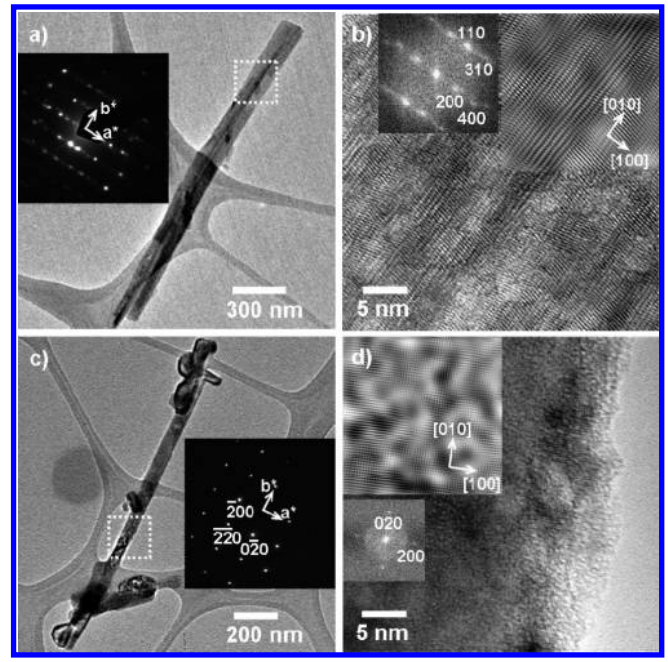

Figure 5. (a) TEM (inset: selected area electron diffraction (SAED) pattern from square marked part) and (b) HRTEM images (insets: Fourier-transformed (FT) and reversed-FT results) of **HA-1** viewing along [001]. (c) TEM (inset: SAED pattern from square marked part) and (d) HRTEM images (insets: FT and reversed-FT results) of **HA-2** viewing along [001].

(29) Bleif, H.-J.; Dachs, H. *Acta Crystallogr., Sect. A* **1982**, *38*, 470.

Table 2. Summary of XRD Relative Intensities, $I_{(hkl)}/I_{(hkl)\mathrm{ref}}$ Together with Photocatalytic Property of the Samples

sample	$I_{(101)}/I_{(101)\mathrm{ref}}$[a]	$I_{(004)}/I_{(004)\mathrm{ref}}$[a]	$I_{(200)}/I_{(200)\mathrm{ref}}$[a]	r_0 (ppm min^{-1})[b]
HA-1				0.2
HA-2	1.1	1.4	1.36	0.5
HB-1				0.6
HB-2	1.06	1.72	1.42	2.0
TiO_2 nanotube	0.83	0.94	1.13	1.0
P25	0.93	1.23	1.13	1.5

[a] Ratios of the XRD intensities of chosen anatase planes normalized to nonoriented anatase, JCPDS 89−4921. [b] Initial reaction rate estimated in first step of the photodecomposition.

active site number in the [010] and [100] directions might explain the differences observed in photocatalytic properties.

Beside the morphology, the crystallographic quality of nanocrystallites also impacts the properties. Recently, TiO_2 nanotubes obtained from the soft-chemical synthesized sodium titanate nanotubes have been reported.[8] We also studied this material and found that its properties were different from those of the nanowires. The TEM and XRD (Figure S9 in the Supporting Information) show that the nanotubes after proton exchange maintained the tubular morphology but the wall structure became less ordered. The highly strained scroll structure of the nanotube before and after the ion-exchange process appears through a (020) peak broadening in the XRD pattern. The proton-exchanged TiO_2 nanotubes were further annealed at 673 K. As shown in the XRD pattern (Figure S9d in the Supporting Information), the processed material crystallizes as anatase mixed with traces of TiO_2(B). The intensities of (101) and (004) peaks are 13% and 6% lower while that of (200) is 13% higher than the nonoriented anatase. This suggests that the anatase TiO_2 processed from the nanotubes may have numerous stacking faults in the (020) planes and a slightly preferential orientation along (100).

3.3.5. TiO_2(B) to Anatase Phase Transformation. In comparison to the literature, the transformation of TiO_2(B) to anatase, which generally occurs at $T = 823$ K[13,14,30] as for the **HB-1** to **HB-2**, takes place at 1073 K for the **HA-1** to **HA-2**. The indicated temperatures refer to the $m = 44$ peak observed by MS (Figures S2c and S2d in the Supporting Information) and attributed to CO_2 departure. A major difference between our work and previous ones mainly lies in the size of the fibers. The classical synthesis leads to micrometric crystallites: 0.25−0.7 μm wide; 1−5 μm long, whereas small or large nanowires are formed by the low temperature process. In addition, the transformation is associated with the release of carbonate groups (probably bidentate), as observed by TGA/MS experiments (Figures S2c and S2d in the Supporting Information). Such an observation may indicate that these adsorbed species also play a critical role in the solid state crystal transformation. Therefore, the same analysis (TGA/MS) was performed on micrometric fibers of TiO_2(B). It clearly appears that the latter contains also some amount of carbonates, suggesting that the stability of TiO_2(B) could be assigned to linked carbonate groups on the crystallite surface which may stabilize the TiO_2(B) surface and create an additional barrier which hampers the phase transformation process toward anatase. However, the higher thermal stability of the present **HA-1** TiO_2(B) can be attributed both to the presence of carbonate and to the size and morphology of the crystallites. This conclusion is further supported by the fact that the quantity of carbonate molecules decreases as the size of the crystallites increases. The transition from TiO_2(B) to anatase occurs at a lower temperature for **HB-1** small nanowires with largest surface area (71 m^2 g^{-1}), whereas the higher one is observed for **HA-1** with large nanowires and smaller surface area value (41 m^2 g^{-1}).

3.4. Structural Reconstruction Mechanism. According to the observations discussed above, we propose a possible mechanism in Scheme 1 to rationalize the formation pathways of the titanates and the TiO_2 compounds. In hot concentrated base solution, the starting TiO_2 particles are dissociated into building blocks composed of linked titanate units. They then recombine into pseudolepidocrocite sodium hydroxo titanate nanowires with the long axis oriented along the *a* direction. This particular arrangement is strongly depending on the Na content, because for lower Na/Ti ratio, the reported Na titanate could not be stabilized. The Na ions in the titanate nanowires can be totally proton exchanged in diluted acid solution and the pseudolepidocrocite structure is retained. After annealing at 673 K, dehydration and condensation of the layered titanic acid convert it into TiO_2(B) nanowires with growth direction along [010] axis. As shown in Scheme 1, the condensation step might proceed via connecting the same colored units after simple shifting of the different colored units. By another simple TiO_6 octahedron migrations shown in the final step in Scheme 1, anatase can be formed from the TiO_2(B) intermediate. The detailed mechanism for the latter phase transformation has been widely studied.[30] The as-prepared anatase crystallizes as nanowires with axis-direction along [010] and exposed (001), (100), (101) planes. The octahedron units migrating in the last step are emphasized by marking them in bold lines. The (001) and defective (101) surfaces were predicted to be photoactive.[3]

Varying the reaction conditions (Table 1) influences the product morphology in many ways. For example, employing amorphous TiO_2, instead of anatase TiO_2, as starting material in the autoclaved process generated thinner diameter sodium titanate nanowires. On the other hand, using anatase TiO_2 in the refluxing process produced sodium titanate nanotubes. The dissociation/dissolution reactions of precursor would be probably more efficient at higher temperature as in autoclave process than that in reflux conditions which operate at lower temperature. Beside this, the sizes of the building blocks, fragmented from the precursor solids, correlate strongly to diameters of the final products. In another case, **B**, which shows analogous phase conversion behavior as **A** does, displays smaller diameters. The reason for this might be the combination of several reaction conditions, such as smaller sized initiator, lower reaction temperature, and lower reaction pressure. From the topotatic condensation of titanate layers proposed in Scheme 1, the thinner nanowires **HB-2** can form, exposing more (001) plane but less of (100) and (101). This

(30) Brohan, L.; Verbaere, A.; Tournoux, M.; Demazeau, G. *Mater. Res. Bull.* **1982**, *17*, 355.

Scheme 1. Proposed Pathway to Convert Bulk Anatase to (001) Plane Exposed Nano-Anatase TiO_2 via Chimie Douce Route by Pseudolepidocrocite Titanate and TiO_2(B) as Intermediate Metaphase; Highlighted Red, Blue, and Black Framed Parts Are the Migrating Units of Condensation

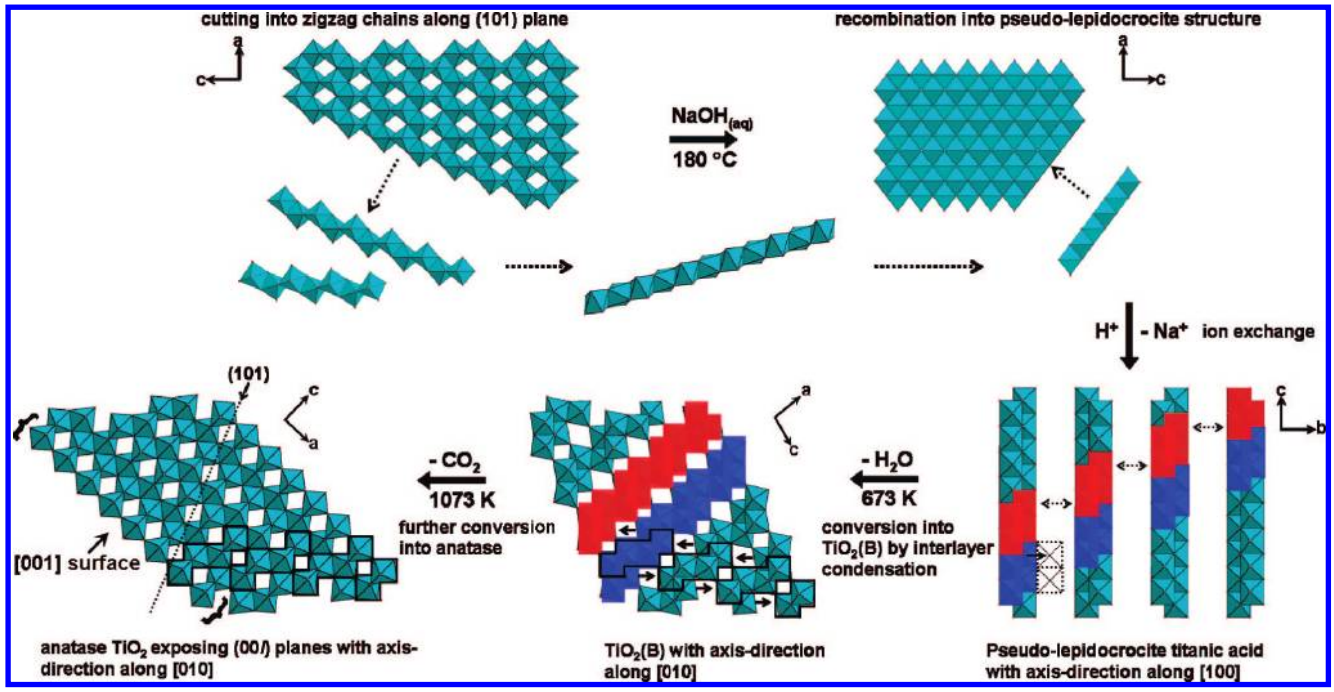

estimation corresponds well with the structural observations of **HA-2** and **HB-2**.

3.5. Photocatalysis Study. Photocatalytic activities of TiO_2(B) nanowires **HA-1**, **HB-1**, anatase nanowires **HA-2**, **HB-2**, TiO_2 from the nanotubes (TiO_2-nanotube) and Degussa P25 nanoparticles were examined in the photodecomposition of an aqueous solution of 25 ppm methylene blue. The kinetic curves are shown in Figure 6 and the initial reaction rates r_0, in the first step of photodecomposition, are summarized in Table 2. Interestingly, the efficiency of the methylene blue photodecomposition, deduced from r_0 values, decreases in the following order: **HB-2** > P25 > TiO_2-nanotube > **HB-1** > **HA-2** > **HA-1**. **HB-2** displays an efficiency 25 and 75% higher than that of P25 and **HA-2,** respectively. According to the specific surface in Table 1, the surface area of **HB-2** (25 m^2 g^{-1}) is half that of P25 (50 m^2 g^{-1}) and twice that of **HA-2** (13 m^2 g^{-1}). From the previously mentioned observations, in section 3.3.4., **HB-2** and **HA-2** expose more (101), (001), and (100) planes than do other TiO_2 anatase. Although **HA-2** and **HB-2** crystallize as anatase nanowires, **HA-2**, because of its thicker crystallite-size and lower surface area, exhibits less exposed (001) surface planes than **HB-2** does, as deduced from the XRD study. Therefore, the higher activities of **HB-2** can be attributed to more exposed (001) than (100) and (101) surface planes, whereas the good activity of P25 might originate from exposed (001) and (100) planes and its higher surface area. This observation is in agreement with the calculated results, i.e., the (001) surface of anatase is more active than (101).[3] Further investigations in that field are needed to produce larger anatase nanowires with (001) preferential orientation.

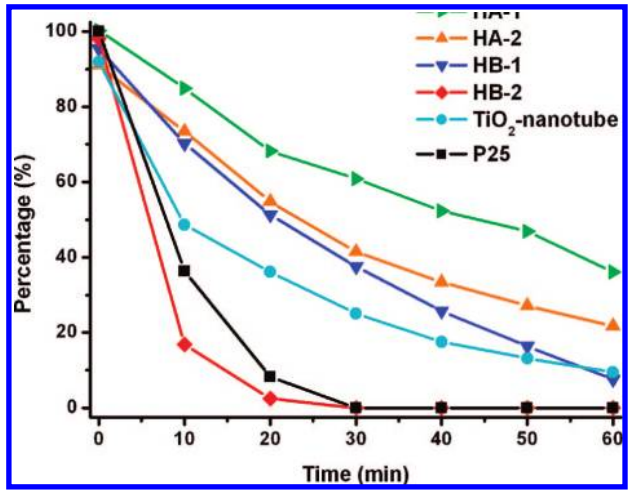

Figure 6. Photocatalytic properties of **HA-1** TiO_2(B) nanowires, **HA-2**, anatase nanorods, **HB-1** small TiO_2(B) nanowires, **HB-2** small anatase nanorods, and TiO_2 from the titanic acid nanotubes compared with Degussa P25 commercial TiO_2 nanoparticles (characterized by decomposing 25 ppm methylene blue aqueous solution under Xe lamp white light radiation).

Even though the TiO_2-nanotube prepared in this study exhibits the highest specific surface area, 323 m^2 g^{-1}, its rather average photocatalytic activity, with r_0 being 1.0 ppm min^{-1}, is lower than those of **HB-2** and P25. The nanotube shows less exposed (001) and (101) surface planes, in addition the inactive (100) surface is more extended than in nonoriented anatase. All the observations mentioned above give a strong experimental evidence and successfully validate the calculated results regarding anatase surface activity[3] and explain why **HB-2** has excellent photocatalytic activity. In future works, to reduce the nanowire thickness will be the key point to improve photocatalytic activity of the products. Although the photocatalytic activity of TiO_2(B) nanowires has been reported to be higher than that of P25 Degussa,[9] in this study, **HA-1** and **HB-1** did not exhibit better efficiency than P25 did.

4. Conclusions

In summary, the structure of $NaTi_2O_4(OH)$ nanowires and derivative products prepared by the alkali method (reflux and autogenous pressure) were studied in details using XRD, ED and HRTEM. Based on density measurements, crystallographic, EDS and TG/MS results, we confirm that the titanate nanowires consist of pseudolepidocrocite arrangement ("$Cs_2Ti_6O_{12}$" type) rather than $Na_2Ti_3O_7$, as previously reported.[31,32] We demonstrated that $NaTi_2O_4(OH)$ exhibits a modulated structure (q wave vector equals 1/7 [001]*), which originates from a misfit between the NaO and $Ti_2O_3(OH)$ sublattices. $NaTi_2O_4(OH)$ structure presents a monoclinic distortion ($I2/m$ space group), with refined parameters $a = 0.37000(6)$ nm, $b = 1.7816(4)$ nm, $c = 2.2077(3)$ nm, and $\beta = 92.70(1)°$. This work contributes to clarify the current controversy on the structures of Na-titanates nanowires. Proton exchange of $NaTi_2O_4(OH)$ followed by heat treatment converts it into titanium dioxide nanowires with $TiO_2(B)$ and then anatase structures. The proposed mechanism of anatase nanostructure formation elucidates the relationship between 2D and 3D nanowire structures. The long axis of the anatase nanowires oriented along the [010] direction and the (001) preferential orientation was explained by a topotactic phase transformation of $TiO_2(B)$ into anatase. The length and thickness of nanowires along (100) can be controlled by adjusting the reaction temperature. The higher photoactivity of anatase TiO_2 nanowires, produced by reflux process, originates from the (001) preferential orientation, despite its lower surface area, as compared to P25. In future works, to reduce the nanowire thickness will be the key point to improve photocatalytic activity of the products.

Acknowledgment. We thank A. Barreau, Service commun de microscopies, Faculté des Sciences, Nantes, for help with SEM studies; P.-E. Petit for XRD studies, E. Gautron for TEM operations; S. Grolleau for TGA/MS measurements; J.-Y. Mevellec for Raman operations; and S. Lefrant for financial support in TEM experiments. We also thank the Institut Français de Taipei and National Chiao Tung University for scholarship support. Financial support from CNRS, France, and NSC, Taiwan, the Republic of China, are gratefully acknowledged.

Supporting Information Available: TGA/MS, FT-IR, Raman, and XRD of **A** and **H-A** (PDF). This material is available free of charge via the Internet at http://pubs.acs.org.

CM8007039

(31) Bavykin, D.-V.; Friedrich, J.-M.; Walsh, F.-C. *Adv. Mater.* **2006**, *18*, 2807.
(32) Morgado, E.-J.; de Abreu, M.-A.-S.; Moure, G.-T.; Marinkovic, B.-A.; Jardim, P.-M.; Araujo, A.-S. *Chem. Mater.* **2007**, *19*, 665.